

Differentiating primary CNS lymphoma from glioblastoma multiforme: assessment using arterial spin labeling, diffusion-weighted imaging, and ^{18}F -fluorodeoxyglucose positron emission tomography

Koji Yamashita · Takashi Yoshiura · Akio Hiwatashi · Osamu Togao · Koji Yoshimoto · Satoshi O. Suzuki · Koichiro Abe · Kazufumi Kikuchi · Yasuhiro Maruoka · Masahiro Mizoguchi · Toru Iwaki · Hiroshi Honda

Received: 31 May 2012 / Accepted: 27 August 2012 / Published online: 9 September 2012
© Springer-Verlag 2012

Abstract

Introduction Our purpose was to evaluate the diagnostic performance of arterial spin labeling (ASL) perfusion imaging, diffusion-weighted imaging (DWI), and ^{18}F -fluorodeoxyglucose positron emission tomography (FDG-PET) in differentiating primary central nervous system lymphomas (PCNSLs) from glioblastoma multiformes (GBMs).

Methods Fifty-six patients including 19 with PCNSL and 37 with GBM were retrospectively studied. From the ASL data, an absolute tumor blood flow (aTBF) and a relative tumor blood flow (rTBF) were obtained within the enhancing portion of each tumor. In addition, the minimum apparent diffusion coefficient (ADC_{min}) and the maximum standard uptake value (SUV_{max}) were obtained from DWI and FDG-PET data, respectively. Each of the four parameters was compared between PCNSLs and GBMs using

Kruskal–Wallis test. The performance in discriminating between PCNSLs and GBMs was evaluated using the receiver-operating characteristics analysis. Area-under-the-curve (AUC) values were compared among the four parameters using a nonparametric method.

Results The aTBF, rTBF, and ADC_{min} were significantly higher in GBMs (mean aTBF \pm SD=91.6 \pm 56.0 mL/100 g/min, mean rTBF \pm SD=2.61 \pm 1.61, mean ADC_{min} \pm SD=0.78 \pm 0.19 $\times 10^{-3}$ mm²/s) than in PCNSLs (mean aTBF \pm SD=37.3 \pm 10.5 mL/100 g/min, mean rTBF \pm SD=1.24 \pm 0.37, mean ADC_{min} \pm SD=0.61 \pm 0.13 $\times 10^{-3}$ mm²/s) ($p < 0.005$, respectively). In addition, SUV_{max} was significantly lower in GBMs (mean \pm SD=13.1 \pm 6.34) than in PCNSLs (mean \pm SD=22.5 \pm 7.83) ($p < 0.005$). The AUC for aTBF (0.888) was higher than those for rTBF (0.810), ADC_{min} (0.768), and SUV_{max} (0.848), although their difference was not statistically significant.

Conclusion ASL perfusion imaging is useful for differentiating PCNSLs from GBMs as well as DWI and FDG-PET.

K. Yamashita · T. Yoshiura (✉) · A. Hiwatashi · O. Togao · K. Abe · K. Kikuchi · Y. Maruoka · H. Honda
Department of Clinical Radiology, Graduate School of Medical Sciences, Kyushu University,
3-1-1, Maidashi, Higashi-ku,
Fukuoka 812-8582, Japan
e-mail: tyoshiu@radiol.med.kyushu-u.ac.jp

K. Yoshimoto · M. Mizoguchi
Department of Neurosurgery, Graduate School of Medical Sciences, Kyushu University,
3-1-1, Maidashi, Higashi-ku,
Fukuoka 812-8582, Japan

S. O. Suzuki · T. Iwaki
Department of Neuropathology, Graduate School of Medical Sciences, Kyushu University,
3-1-1, Maidashi, Higashi-ku,
Fukuoka 812-8582, Japan

Keywords Arterial spin labeling · Glioblastoma · Primary CNS lymphoma

Introduction

Primary central nervous system lymphoma (PCNSL) is less common than gliomas, the incidence of which is increasing in both immunosuppressed and immunocompetent individuals [1–5]. PCNSLs are usually treated by chemotherapy and whole brain radiotherapy, without extended surgical mass reduction. Target biopsy is sufficient for pathological diagnosis in most cases.

On the other hand, glioblastoma multiforme (GBM) is the most common primary malignant brain tumor in adults with a rapid and highly infiltrative growth. In the vast majority of cases with a clinically and radiographically suspected GBM, gross surgical resection is attempted. Once the pathological diagnosis of GBM is made, it is most often followed by a chemoradiotherapy using temozolomide [6, 7]. Therefore, pretreatment differentiation between PCNSL and GBM is essential for therapeutic decision-making.

The magnetic resonance (MR) imaging characteristics of PCNSL and GBM have been well-documented in the literature [1, 8]. Although conventional MR techniques including postcontrast T1-weighted images are useful in the discrimination of these tumors, there is a considerable overlap in their features: both are usually manifested as strongly enhancing masses, often accompanied by surrounding edema. Previous reports have shown that several functional imaging parameters are useful for this purpose, including the apparent diffusion coefficient (ADC) derived from diffusion-weighted MR imaging (DWI), tumor blood volume (TBV) calculated from the dynamic susceptibility contrast (DSC) perfusion MR imaging, and the standardized uptake value (SUV) from ^{18}F -fluorodeoxyglucose positron emission tomography (FDG-PET) [2, 3, 9–16].

Arterial spin labeling (ASL) is an emerging MR perfusion imaging technique that utilizes magnetically labeled arterial blood as an intrinsic tracer. It is increasingly recognized as a noninvasive method for quantitative cerebral blood flow (CBF) measurement in the assessment of stroke, neurodegenerative diseases, and brain tumors [17–26]. At present, the gold standard of regional CBF analysis is ^{15}O -PET study.

However, in cerebral gliomas, Tyler et al. reported that measurements of CBF using ^{15}O -PET may be inaccurate due to low spatial resolution and quantitative artifacts [27]. We hypothesized that perfusion imaging with ASL could be useful in discriminating PCNSLs from GBMs. To test our hypothesis, we evaluated the diagnostic performance of ASL compared to those of DWI and FDG-PET.

Materials and methods

Subjects

This study was approved by the institutional review board of our hospital. Informed consent for study participation was waived due to the retrospective nature of this study.

MR imaging data of the consecutive patients obtained between January 2008 and September 2011 were retrospectively analyzed. A total of 56 patients including 19 with PCNSL (mean age 64.8 ± 10.5 years; age range 42–79 years) and 37 with GBM (mean age 58.5 ± 16.7 years; age range 8–

83 years) were identified. Among them, ASL was performed in 12 patients with PCNSL and 35 with GBM, DWI was performed in 17 with PCNSL and 37 with GBM, and FDG-PET was performed in 16 with PCNSL and 24 with GBM. Fifteen patients with PCNSL were histologically diagnosed by stereotactic biopsy or surgical resection. The remaining four cases were recurrent PCNSLs that were diagnosed based on clinical and radiological information. All GBMs were histopathologically diagnosed. In all subjects, both MR imaging and FDG-PET were obtained before treatment. The mean time interval between MR imaging and FDG-PET was 1.5 days (range 0–6 days).

MR imaging

All images were obtained using a 3.0-T MR imaging unit (Achieva Quasar Dual, Philips Medical Systems, Best, Netherlands) and an eight-channel head array receiving coil for sensitivity encoding (SENSE) parallel imaging.

Arterial spin labeling

ASL was performed by using Quantitative STAR labeling of Arterial Region (QUASAR), a pulsed ASL technique developed by Petersen et al. [28]. QUASAR was designed to allow for quantitative measurement of CBF by minimizing the effect of arterial transit delay of labeled blood. To achieve this goal, multi-inversion delay sampling based on the Look-Locker technique is implemented so that the time course of post-labeling perfusion-related signal intensity change in each imaging voxel can be estimated [29]. Our QUASAR protocol consisted of 84 dynamics or 42 pairs of labeled and nonlabeled image acquisitions. Out of these, 24 pairs were acquired with crusher gradients (velocity encoding= $[\infty, 4 \text{ cm/s}]$) and 12 pairs were acquired without crushers. These 36 pairs were acquired at a flip angle of 35° . An additional six pairs were acquired at a lower flip angle (11.7°) without crushers to estimate the actual flip angle that might vary across the brain due to inhomogeneity of B1. Other imaging parameters were as follows: labeling slab thickness=150 mm, gap between the labeling and imaging slabs=15 mm, SENSE factor=2.5, TR/TE=4,000/22 ms, sampling interval=300 ms, sampling time points=13, field of view (FOV)=240 mm, matrix size= 64×64 , and imaging time=5 min 52 s. Seven 6-mm-thick transverse slices (gap=2 mm) were placed to cover the tumor.

Diffusion-weighted imaging

DWI was performed using a single-shot spin-echo (SE) echo-planar sequence with the following parameters: TR/TE=3,421/62 ms, 90° flip angle, NEX=1, 22 transverse sections, SENSE factor=2.5, slice thickness/gap=5 mm/

1 mm, FOV=230 mm, 126×160 matrix, and imaging time of 44.5 s. Diffusion sensitizing gradients were applied sequentially in the *x*, *y*, and *z* directions with *b* factors of 0 and 1,000 s/mm².

Conventional MR imaging

Postcontrast transverse T1-weighted SE images (TR/TE=400/10 ms, 75° flip angle, NEX=1, 22 sections, slice thickness/gap=5 mm/1 mm, FOV=230 mm, 256×173 matrix) were obtained. A standard dose (0.1 mmol/kg body weight) of a Gd-based contrast agent (Magnevist, Bayer Schering Pharma AG, Berlin, Germany) was injected intravenously. Precontrast T1-weighted SE, T2-weighted turbo SE images, and fluid-attenuated inversion recovery images were also obtained.

FDG-PET

Data acquisition was performed with a PET/CT Discovery STE system (GE Healthcare, Milwaukee, WI, USA) for 8 cases with PCNSL and 11 with GBM, and with a Biograph mCT system (Siemens AG, Erlangen, Germany) for 8 cases with PCNSL and 13 with GBM. Both systems produce transverse, coronal, and sagittal reconstructions of CT, PET, and fusion PET/CT data for interpretation.

Patients fasted for at least 4 h before FDG administration, and 185 MBq of FDG (FDG Injectable; Nihon Medi-Physics, Tokyo, Japan) was intravenously administered to each patient. Images were acquired 1 h after FDG administration.

The Discovery STE scanner consists of a 16-slice multi-detector CT and bismuth germinate oxide crystal. The unenhanced CT was performed first at 120 kVp and 150 mA, and then, the PET images were obtained in 3D mode for 8 min on a single bed position with an axial FOV of 30 cm in a 128×128 matrix. Based on the CT data, transmission maps were created and used for attenuation correction of the PET images. The PET data were reconstructed using the iterative ordered subsets expectation maximization algorithm (VUE Point Plus) with 2 iterations and 28 subsets. The Biograph mCT scanner is equipped with a 128-slice multidetector CT and lutecium silicate oxide crystal. The noncontrast-enhanced CT was performed at 120 kVp and 160 mA. The PET images were obtained in 3D mode for 10 min on a single bed position with an axial FOV of 40 cm in a 400×400 matrix. The concomitant CT data were used for attenuation correction. The PET data were reconstructed using a 3D ordered subset expectation maximization algorithm with 8 iterations and 21 subsets. TOF and point spread function techniques were also used for the image reconstruction (ultra HD-PET).

Image analysis

The ASL data were analyzed on a desktop computer (Panasonic Corporation, Osaka, Japan). Maps of CBF were obtained by using dedicated software running on IDL (Research Systems, Boulder, CO, USA), which was developed and provided by Petersen (National Neuroscience Institute, Singapore). Measurement of blood flow was performed using a region-of-interest (ROI) analysis by the consensus of the two neuroradiologists (KY and OT) who were blinded to the clinical and pathologic information. A free software package (MRicro, Chris Rorden) was used to draw ROIs on the CBF maps. For each tumor, a mean absolute tumor blood flow (aTBF) was measured in a ROI that was drawn over the enhancing area on the single slice with the largest cross-sectional area. Pre- and postcontrast-enhanced T1-weighted images were used as anatomical references [30]. Careful attention was paid to avoid contamination of blood vessels, calcification, necrosis, and hemorrhage. In addition, a relative tumor blood flow (rTBF) was obtained by normalizing the aTBF by a blood flow measurement from the reference region based on previous reports [30–33]. Specifically, a cluster of more than 10 voxels was selected in the normal appearing cortical gray matter in the contralateral hemisphere as a reference region on the same slice as the ROI for the tumor in all cases.

Maps of ADC were calculated using the following formula: $\ln(S/S_0) = -b \times \text{ADC}$, where S_0 and S are the signal intensities when the *b* values are 0 and 1,000 s/mm², respectively, and *b* itself is 1,000 s/mm². For ADC measurements, one author (KY) performed the ROI analysis using a picture archiving and communication system (Rapideye, Toshiba, Tochigi, Japan). Ten or more circular ROIs (area=10 mm²) were placed on ADC maps within the area that corresponded to the enhancing area on postcontrast T1-weighted images, and the mean ADC value was obtained for each ROI. Regions with relatively low ADC were targeted, while blood vessels, calcification, necrosis, and hemorrhage were strictly avoided for ROIs placement. The lowest ADC value chosen from all placed ROIs was determined as the minimum ADC (ADCmin).

Reconstructed PET data were converted to SUV data using the following equation: SUV = activity at a pixel (kBq/cm³)/injection dose (MBq)/weight (kg). The maximum standardized uptake value (SUVmax) of the tumor was identified by establishing a volume of interest over the enhancing area on the MR image. Pre- and postcontrast T1-weighted images were used as anatomical references.

The aTBF, rTBF, ADCmin, and SUVmax values were compared between PCNSLs and GBMs using the Kruskal–Wallis test at the significance level of $p < 0.05$. The sensitivity, specificity, and accuracy for the discrimination between PCNSLs and GBMs were calculated with each parameter

using an optimal cut-off value determined by the receiver-operating characteristics (ROC) analysis. Area-under-the-ROC curve (AUC) values for the discrimination were calculated for the four parameters. AUC values were compared with each other using a nonparametric approach [34].

In addition, a logistic analysis was used to determine whether any pair-wise combination of the four parameters could increase the diagnostic performance. For this analysis, only patients who underwent both of the two modalities of interest were taken into account: 12 PCNSLs and 35 GBMs for ASL versus ADC, 7 PCNSLs and 26 GBMs for ASL versus FDG-PET, and 12 PCNSLs and 26 GBMs for ADC versus FDG-PET. Statistical analyses were performed using JMP 8 software (SAS Institute, Cary, NC, USA).

Results

Figure 1 shows plots of aTBF, rTBF, ADCmin, and SUVmax in PCNSLs and GBMs. The aTBF, rTBF, and ADCmin values were significantly higher in GBMs (mean aTBF \pm SD=91.6 \pm 56.0 mL/100 g/min, mean rTBF \pm SD=2.61 \pm

1.61, mean ADCmin \pm SD=0.78 \pm 0.19 $\times 10^{-3}$ mm²/s) than in PCNSLs (mean aTBF \pm SD=37.3 \pm 10.5 mL/100 g/min, mean rTBF \pm SD=1.24 \pm 0.37, mean ADCmin \pm SD=0.61 \pm 0.13 $\times 10^{-3}$ mm²/s) ($p<0.005$, respectively). In addition, the SUVmax value was significantly lower in GBMs (mean \pm SD=13.1 \pm 6.34) than in PCNSLs (mean \pm SD=22.5 \pm 7.83) ($p<0.005$). Figures 2, 3, and 4 show illustrative cases.

The optimal cut-off value was 46 mL/100 g/min for aTBF with 83.3 % sensitivity, 82.9 % specificity, and 83.0 % accuracy. For rTBF, the optimal cut-off value was 1.25 with 58.3 % sensitivity, 82.9 % specificity, and 76.6 % accuracy. For ADCmin, the optimal cut-off value was 0.62 $\times 10^{-3}$ mm²/s with 58.8 % sensitivity, 86.5 % specificity, and 77.8 % accuracy. Finally, the optimal cut-off value was 19.0 for SUVmax with 92.3 % sensitivity, 79.2 % specificity, and 83.8 % accuracy. The AUC values for the aTBF, rTBF, ADCmin, and SUVmax were 0.888, 0.810, 0.768, and 0.848, respectively. No significant difference in AUC values was found among the four measurements. Figure 5 shows the ROC curves for the four measurements. No pair-wise combination of the four measurements resulted in an increased AUC value (Table 1).

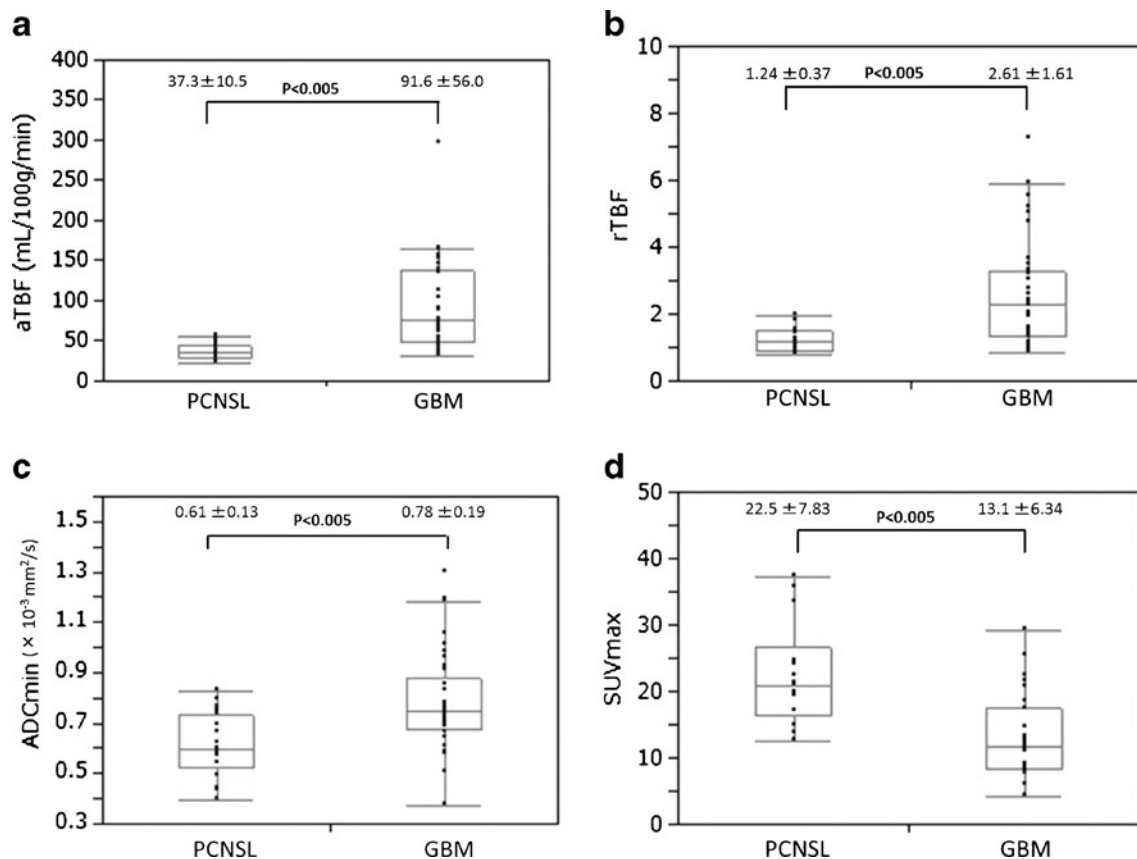
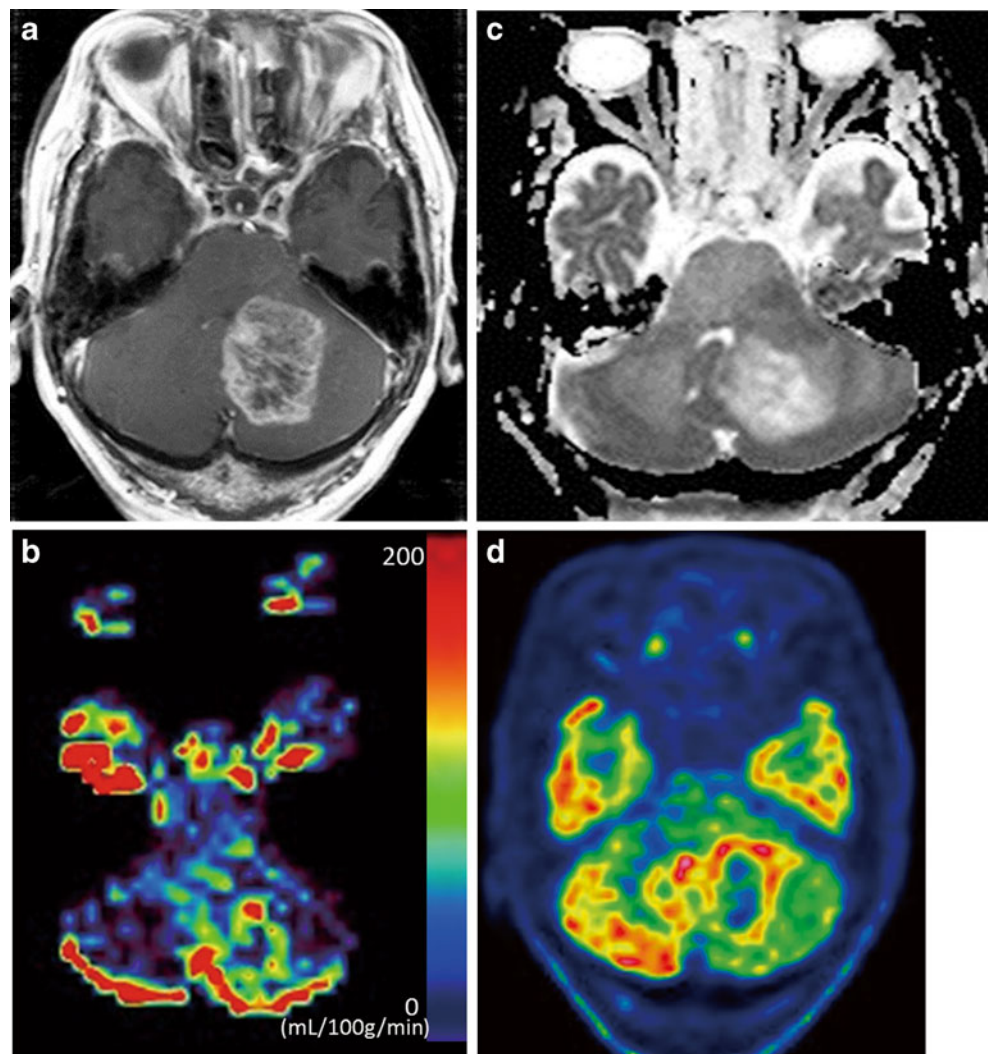


Fig. 1 Plots of aTBF (a), rTBF (b), ADCmin (c), and SUVmax (d) in PCNSLs and GBMs. The aTBF, rTBF, and ADCmin values are significantly higher in GBMs in comparison with PCNSLs ($p < 0.005$,

respectively). In addition, SUVmax value is significantly lower in GBMs in comparison with PCNSLs ($p < 0.005$)

Fig. 2 A contrast-enhanced T1WI (a), aTBF map derived from ASL (b), ADC map derived from DWI (c), and FDG-PET (d) of a 83-year-old female with GBM. High aTBF (144 mL/100 g/min) and rTBF (5.02) are demonstrated in the enhancing tumor. The tumor shows high ADCmin ($0.83 \times 10^{-3} \text{ mm}^2/\text{s}$) and relatively low SUVmax (11.9)



Discussion

Several previous reports have shown that PCNSL is associated with lower ADC than GBM [9–12], and our result was consistent with those reports (Fig. 1). Histologically, PCNSL has high cellularity and the tumor cells infiltrate the brain parenchyma either as individual diffusely infiltrating cells or as compact aggregates of tightly packed cells [3], which may result in low ADC on DWI. Doskaliyev et al. [11] and Calli et al. [12] reported that PCNSL can be discriminated from GBM based on ADCmin with a high level of accuracy.

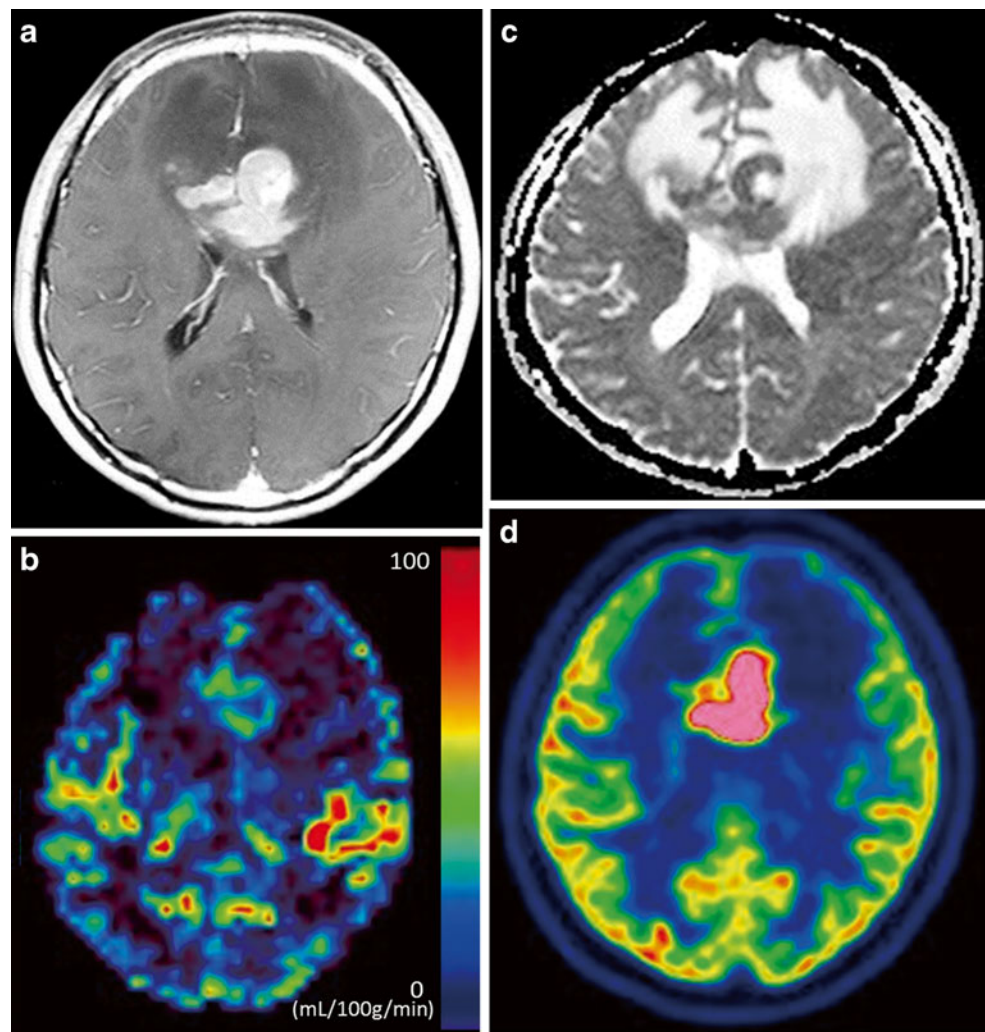
Our FDG-PET result showed higher SUVmax in PCNSLs than in GBMs, which is consistent with previous reports [15, 16]. The higher SUVmax in PCNSLs than in GBMs may correspond to the higher cell density and/or higher glucose consumption rate of tumor cells in the former [15, 16, 35].

Vascularity is another parameter that is known to distinguish PCNSLs from GBMs. Previous studies based on DSC

perfusion imaging have shown that GBMs are associated with higher TBV than are PCNSLs [12–14]. Pathophysiologically, this may be attributed to the blood–brain barrier destruction with neovascularization in GBMs, while without neovascularization in PCNSLs [2, 12–14]. ASL is an alternative method of MR perfusion imaging that has been used to assess the vascularity of brain tumors. It has been reported to be useful in evaluating vascularity in meningiomas, in differentiating hemangioblastomas from metastatic brain tumors, and in evaluating high- versus low-grade gliomas [17, 23–25, 30, 36]. However, ASL findings in PCNSLs have rarely been reported. Our study demonstrated that ASL blood flow measurement is useful for distinguishing PCNSLs from GBMs. Both aTBF and rTBF were significantly higher in GBMs than in PCNSLs (Fig. 1), which is consistent with the TBV results from DSC perfusion imaging studies [12–14].

There has been no study that compared diagnostic performance of different imaging modalities in discriminating PCNSLs and GBMs. We found that ASL performed as well

Fig. 3 A contrast-enhanced T1WI (**a**), aTBF map derived from ASL (**b**), ADC map derived from DWI (**c**), and FDG-PET (**d**) of a 43-year-old male with PCNSL. ASL perfusion demonstrates relatively low aTBF (52.0 mL/100 g/min) in the enhancing tumor. The tumor shows low ADCmin ($0.66 \times 10^{-3} \text{ mm}^2/\text{s}$) and high SUVmax (35.5)



as DWI and FDG-PET. Especially, when aTBF was used, ASL was associated with a higher AUC value (0.888) than that of DWI (0.768) or FDG-PET (0.848), although the difference was not statistically significant.

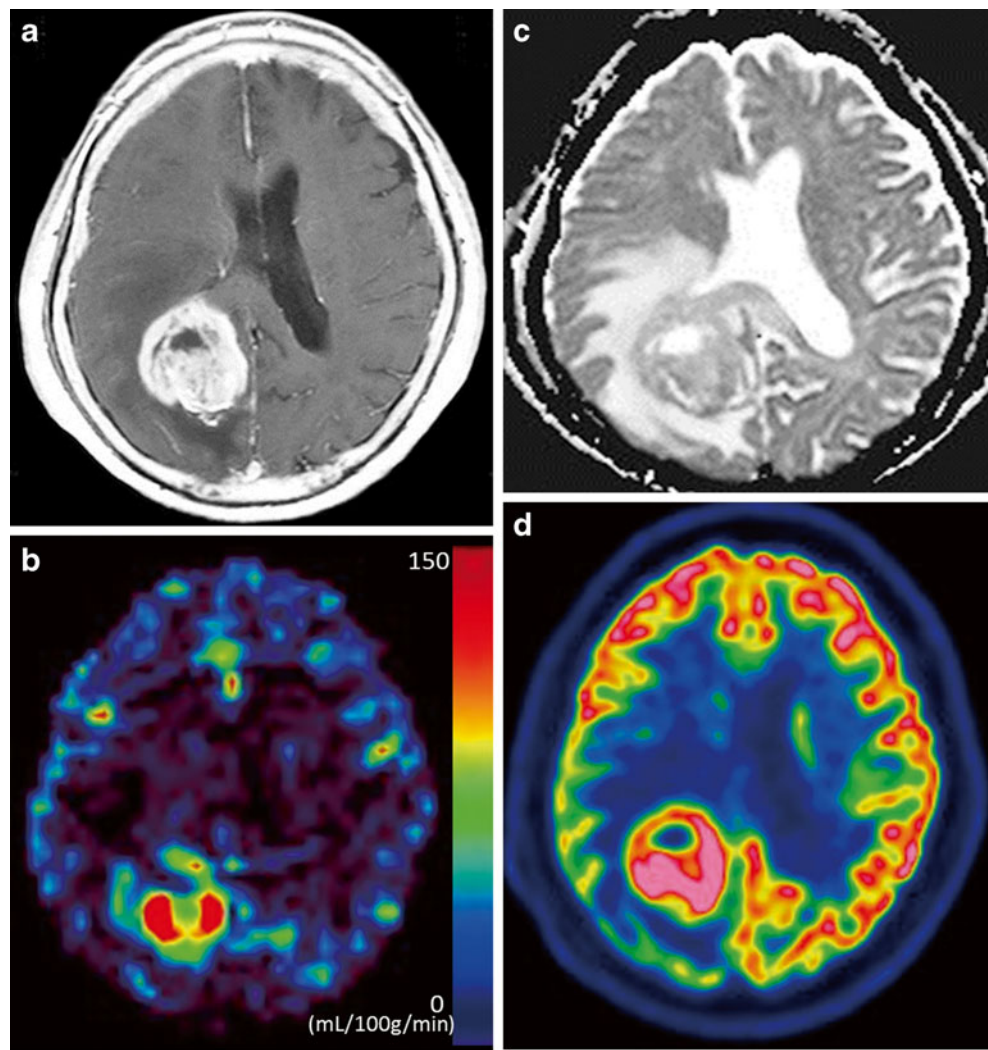
ASL requires no extrinsic tracer or radiation exposure. These features are advantages of ASL over FDG-PET and DSC perfusion imaging. Moreover, the typical imaging time of ASL is 5 to 6 min. Thus, it can be easily performed along with other conventional MR imaging techniques. Although DSC perfusion imaging has been more widely used to assess brain tumors, Lehmann et al. revealed that ASL provided similar information to DSC perfusion imaging for relative CBF measurement in brain tumors [30]. Compared to DSC perfusion imaging, ASL is less ambiguous regarding the contribution of permeability and blood flow to the signal intensity. Results of DSC perfusion imaging can be distorted by the T2* and T1 effects due to the contrast agent leakage from the local tumor vasculatures. On the other hand, the signal intensity of ASL is considered to be directly proportional to the blood flow [37]. This may not be true in tumor

patients due to a different microvascular architecture between normal and tumor tissue. Nevertheless, our results indicated that ASL provides valuable diagnostic information to distinguish PCNSLs and GBMs.

There was a wide variability in aTBF among GBMs, while the variability among PCNSLs appeared very small (Fig. 1). This may reflect a true variability in the vascularity among GBMs, or it may have been due to the partial volume effect in ASL blood flow measurement. Typically, the spatial resolution of ASL is limited, as shown in our study (imaging voxel size = $3.75 \times 3.75 \times 8 \text{ mm}^3$). This might have resulted in the underestimation of aTBF, especially when the enhancing compartment of the tumor was demonstrated as a thin ring-like enhancement. It should be noted that differentiation of PCNSLs and GBMs by ASL is difficult in such cases.

We found no particular benefit of making a pair-wise combination of the four imaging parameters (Table 1). Obviously, this is at least in some part due to the different

Fig. 4 A contrast-enhanced T1WI (a), aTBF map derived from ASL (b), ADC map derived from DWI (c), and FDG-PET (d) of a 81-year-old female with GBM. High aTBF (151 mL/100 g/min) and rTBF (5.87) are demonstrated in the enhancing tumor. However, the tumor shows low ADCmin ($0.69 \times 10^{-3} \text{ mm}^2/\text{s}$) and high SUVmax (29.2) which are comparable to those in PCNSL



number of patients who underwent the respective combinations of modalities (see the description in “Materials and methods”). Further studies with setting a strict standard for subjects may reveal combinations of different modalities that improve the diagnostic performance. Furthermore, it

might result in advancement of the prediction of response to therapy and the differential diagnosis between tumor recurrence and necrosis.

Our study had several limitations. First, as mentioned earlier, not all patients were studied by the three imaging modalities (ASL, DWI, and FDG-PET). Some cases of PCNSLs were diagnosed without pathological confirmation.

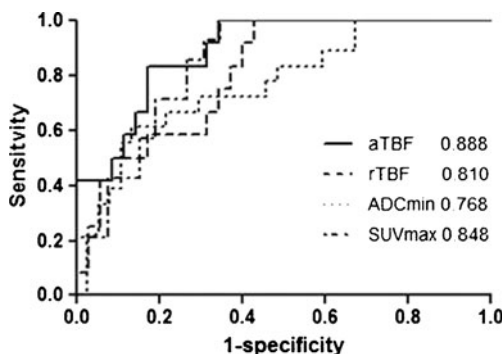


Fig. 5 The ROC curves for the discrimination between PCNSLs and GBMs by aTBF, rTBF, ADCmin, and SUVmax

Table 1 Pair-wise combination of aTBF, rTBF, ADCmin, and SUVmax

Measurements	AUC value
aTBF, ADCmin	0.700
aTBF, SUVmax	0.579
rTBF, AUCmin	0.706
rTBF, SUVmax	0.553
AUCmin, SUVmax	0.486

Note: The combination of the aTBF and rTBF was excluded

PCNSL cases were less than half the number compared to GBM. Data of DSC perfusion imaging were not available.

Conclusion

Our results suggested that ASL perfusion imaging is useful for differentiating PCNSLs from GBMs as well as DWI and FDG-PET.

Acknowledgments This work was supported by JSPS KAKENHI Grant Number 23791432.

Conflict of interest We declare that we have no conflict of interest.

References

- Koeller KK, Smirniotopoulos JG, Jones RV (1997) Primary central nervous system lymphoma: radiologic–pathologic correlation. *RadioGraphics* 17:1497–1526
- Cha S, Knopp EA, Johnson G, Wetzel SG, Litt AW, Zagzag D (2002) Intracranial mass lesions: dynamic contrast-enhanced susceptibility-weighted echo-planar perfusion MR imaging. *Radiology* 223:11–29
- Guo AC, Cummings TJ, Dash RC, Provenzale JM (2002) Lymphomas and high-grade astrocytomas: comparison of water diffusibility and histologic characteristics. *Radiology* 224:177–183
- Morris PG, Abrey LE (2009) Therapeutic challenges in primary CNS lymphoma. *Lancet Neurol* 8:581–592
- Lee IH, Kim ST, Kim HJ, Kim KH, Jeon P, Byun HS (2010) Analysis of perfusion weighted image of CNS lymphoma. *Eur J Radiol* 76:48–51
- National Comprehensive Cancer Network clinical practice guidelines in oncology—central nervous system cancers. v.1.2010. [http://www.nccn.org/professionals/physician_gls/PDF/cns.pdf]. Accessed Dec 2011
- Stupp R, Mason WP, van den Bent MJ et al (2005) Radiotherapy plus concomitant and adjuvant temozolomide for glioblastoma. *N Engl J Med* 352:987–996
- Rees JH, Smirniotopoulos JG, Jones RV, Wong K (1996) Glioblastoma multiforme: radiologic–pathologic correlation. *RadioGraphics* 16:1413–1438
- Yamasaki F, Kurisu K, Satoh K et al (2005) Apparent diffusion coefficient of human brain tumors at MR imaging. *Radiology* 235:985–991
- Toh CH, Castillo M, Wong AM et al (2008) Primary cerebral lymphoma and glioblastoma multiforme: differences in diffusion characteristics evaluated with diffusion tensor imaging. *AJNR Am J Neuroradiol* 29:471–475
- Doskaliyev A, Yamasaki F, Ohtaki M et al (2012) Lymphomas and glioblastomas: differences in the apparent diffusion coefficient evaluated with high *b*-value diffusion-weighted magnetic resonance imaging at 3 T. *Eur J Radiol* 81:339–344
- Calli C, Kitis O, Yuntun N, Yurtseven T, Islekel S, Akalin T (2006) Perfusion and diffusion MR imaging in enhancing malignant cerebral tumors. *Eur J Radiol* 58:394–403
- Hartmann M, Heiland S, Harting I et al (2003) Distinguishing of primary cerebral lymphoma from high-grade glioma with perfusion-weighted magnetic resonance imaging. *Neurosci Lett* 338:119–122
- Hakyemez B, Erdogan C, Bolca N, Yildirim N, Gokalp G, Parlak M (2006) Evaluation of different cerebral mass lesions by perfusion-weighted MR imaging. *J Magn Reson Imaging* 24:817–824
- Kosaka N, Tsuchida T, Uematsu H, Kimura H, Okazawa H, Itoh H (2008) 18F-FDG PET of common enhancing malignant brain tumors. *AJR Am J Roentgenol* 190:W365–W369
- Makino K, Hirai T, Nakamura H et al (2011) Does adding FDG-PET to MRI improve the differentiation between primary cerebral lymphoma and glioblastoma? Observer performance study. *Ann Nucl Med* 25:432–438
- Warmuth C, Gunther M, Zimmer C (2003) Quantification of blood flow in brain tumors: comparison of arterial spin labeling and dynamic susceptibility-weighted contrast-enhanced MR imaging. *Radiology* 228:523–532
- Järnum H, Steffensen EG, Knutsson L et al (2010) MRI of brain tumours: a comparative study of pseudo-continuous arterial spin labelling and dynamic susceptibility contrast imaging. *Neuroradiology* 52:307–317
- Detre JA, Alsop DC, Vives LR et al (1998) Noninvasive MRI evaluation of cerebral blood flow in cerebrovascular disease. *Neurology* 50:633–641
- Chalela JA, Alsop DC, Gonzalez-Atavales JB et al (2000) Magnetic resonance perfusion imaging in acute ischemic stroke using continuous arterial spin labeling. *Stroke* 31:680–687
- Alsop DC, Detre JA, Grossman M (2000) Assessment of cerebral blood flow in Alzheimer's disease by spin-labeled magnetic resonance imaging. *Ann Neurol* 47:93–100
- Yoshiura T, Hiwatashi A, Noguchi T et al (2009) Arterial spin labelling at 3-T MR imaging for detection of individuals with Alzheimer's disease. *Eur Radiol* 19:2819–2825
- Chawla S, Wang S, Wolf RL et al (2007) Arterial spin-labeling and MR spectroscopy in the differentiation of gliomas. *AJNR Am J Neuroradiol* 28:1683–1689
- Kim HS, Kim SY (2007) A prospective study on the added value of pulsed arterial spin-labeling and apparent diffusion coefficients in the grading of gliomas. *AJNR Am J Neuroradiol* 28:1693–1699
- Noguchi T, Yoshiura T, Hiwatashi A et al (2008) Perfusion imaging of brain tumors using arterial spin-labeling: correlation with histopathologic vascular density. *Am J Neuroradiol* 29:688–693
- Tourdias T, Rodrigo S, Oppenheim C et al (2008) Pulsed arterial spin labeling applications in brain tumors: practical review. *Neuro-radiol* 35:79–89
- Tyler JL, Diksic M, Villemure JG et al (1987) Metabolic and hemodynamic evaluation of gliomas using positron emission tomography. *J Nucl Med* 28:1123–1133
- Petersen ET, Lim T, Golay X (2006) Model-free arterial spin labeling quantification approach for perfusion MRI. *Magn Reson Med* 55:219–232
- Look DC, Locker DR (1970) Time saving in measurement of NMR and EPR relaxation times. *Rev Sci Instrum* 41:250–251
- Yamashita K, Yoshiura T, Hiwatashi A et al (2012) Arterial spin labeling of hemangioblastoma: differentiation from metastatic brain tumors based on quantitative blood flow measurement. *Neuroradiology* 54:809–813
- Lehmann P, Monet P, de Marco G et al (2010) A comparative study of perfusion measurement in brain tumours at 3 Tesla MR: arterial spin labeling versus dynamic susceptibility contrast-enhanced MRI. *Eur Neurol* 64:21–26
- Loeber RT, Sherwood AR, Renshaw PF et al (1999) Differences in cerebellar blood volume in schizophrenia and bipolar disorder. *Schizophr Res* 37:81–89
- Löbel U, Sedlacik J, Reddick WE et al (2011) Quantitative diffusion-weighted and dynamic susceptibility-weighted contrast-enhanced perfusion MR imaging analysis of T2 hypointense lesion

- components in pediatric intrinsic pontine glioma. *AJNR Am J Neuroradiol* 32:315–322
34. DeLong ER, DeLong DM, Clarke-Pearson DL (1988) Comparing the areas under two or more correlated receiver operating characteristic curves: a nonparametric approach. *Biometrics* 44:837–845
 35. Herholz K, Pietrzyk U, Voges J et al (1993) Correlation of glucose consumption and tumor cell density in astrocytomas. A stereotactic PET study. *J Neurosurg* 79:853–858
 36. Wolf RL, Wang J, Wang S et al (2005) Grading of CNS neoplasms using continuous arterial spin labeled perfusion MR imaging at 3 Tesla. *J Magn Reson Imaging* 22:475–482
 37. Pfefferbaum A, Chanraud S, Pitel AL et al (2010) Volumetric cerebral perfusion imaging in healthy adults: regional distribution, laterality, and repeatability of pulsed continuous arterial spin labeling (PCASL). *Psychiatry Res* 182:266–273